

Surface morphology and X-ray photoelectron spectroscopy of BiFeO₃ thin films deposited on top of Ta₂O₅/Si layers

*Shikhgasan Ramazanov*¹, *Ștefan Țălu*^{2,*}, *Rashid Dallaev*³, *Guseyn Ramazanov*⁴, *Pavel Škarvada*³, *Jindřich Oulehla*⁵, *Dinara Sobola*^{3,6}, and *Dmitry Nazarov*⁷

¹Dagestan State University, Makhachkala, St. M. Gadjieva 43-a, Dagestan Republic, 367000, Russia

²The Technical University of Cluj-Napoca, The Directorate of Research, Development and Innovation Management (DMCDI), Constantin Daicoviciu Street, no. 15, Cluj-Napoca, 400020, Cluj county, Romania.

³Brno University of Technology, Faculty of Electrical Engineering and Communication, Physics Department, Technická 8, 616 00 Brno, Czech Republic.

⁴Dagestan State Technical University, Makhachkala, St. I. Shamil, 70, Dagestan Republic, 367026, Russia

⁵Institute of Scientific Instruments of the Czech Academy of Sciences, Královopolská 147, 612 64 Brno, Czech Republic

⁶Institute of Physics of Materials, Academy of Sciences ČR, Žižkova 22, 616 62, Brno, Czech Republic

⁷Ural State University of Economics, Institute of management and information technologies, Russian Federation

Abstract. In this study a comparison of the topography of BiFeO₃ (BFO) thin films deposited on tantalum pentoxide substrates of different thicknesses is provided. The Ta₂O₅ substrates had a roughness increasing with the film thickness. The relationship between substrates of different topography but the same composition with the quality of the growing bismuth ferrite film is estimated. For the first time the topography estimation of BFO on Ta₂O₅ is presented. The difference in temperature expansion coefficients leads to intensive evaporation of bismuth ferrite from the surface during annealing. XPS analysis is provided for as-deposited and annealed BFO layers.

1 Introduction

Data storage and processing centers are large consumers of energy resources due to the development of cloud storage services, social networks, mobile applications. The use of new electronic components is a necessary condition for the further growth of capacities and rates of functioning of these resources. Such elements include logical elements of a new type, memristors, which are the basis of non-volatile memory with a high density of

* Corresponding author: stefan_ta@yahoo.com

information storage, etc. Owing to its attractive optical and electrical properties tantalum pentoxide (Ta_2O_5) attracts ever increasing attention of the scientific community nowadays [1]. High dielectric constant and large RI (refractive index) make Ta_2O_5 an excellent candidate to be considered in a number of various applications. For instance, it can serve as an insulating material in all sorts of “sandwich” structures such as MIS (metal/insulator/semiconductor) or MIM (metal/insulator/metal) [2,3]. Another possible application of Ta_2O_5 emerges due to its ability to withstand harsh environments, high temperatures and overall chemical sturdiness/inertness. Therefore, thin films of Ta_2O_5 may also be utilized as protective players in various sensors, detectors and other electronics which might benefit from extra shielding against aggressive media and corrosion. Low absorption coefficient along with large refractive index is absolutely essential when it comes to antireflective coatings which is why Ta_2O_5 find its use in solar cells fabrication as well. Such optical properties are also sought after during manufacture of optical filters and photonic crystals. Biological industry may also benefit from the inclusion of Ta_2O_5 since it has been shown to be a viable choice for production of biochemical and biological sensors and detectors [4,5]. Protein detection and hydrogen ion sensing membranes are some of the examples of these sensors/detectors. Aforementioned were only the explored applications of the Ta_2O_5 but one may already conclude that it is a quite promising material, however, preparation of Ta_2O_5 is a rather challenging procedure. There is great amount of methods which allow obtaining Ta_2O_5 with various degrees of success. Among those methods are methods of chemical vapour deposition (CVD) group: spray pyrolysis, atomic layer deposition, sol-gel methods; and physical vapour deposition (PVD) group: magnetron sputtering, ion assisted coating technique, thermal evaporation coating etc. [6–8]. However due to Ta_2O_5 specific chemical nature a usage sol-gel ablation method is recommended. BFO has a small band gap of ~ 2.8 eV. It is a chemically stable compound. According to the latest literature reports, BFO thin films are utilized as photocatalysts, due to their remarkable photocatalytic activity in the visible light spectrum [9,10]. Other applications of BFO include gas sensors and solar cells [11]. The Ta_2O_5 is also an optical material, and with thin films BFO will allow the use of these compositions in optical magnetic applications. The ALD method makes it possible to obtain 100% conformal films on the surface of substrates, which is relevant to the application of this method in the mentioned applications.

2 Experimental results

The films of BFO composition were prepared by atomic layer deposition (ALD) at ALDCERAM ML-200 device. Samples were obtained by layer-by-layer growth of BiO_x and FeO_x . The source for bismuth component was $Bi(mmp)_3$ and ferrocene was the source of iron $Fe(C_5H_5)_2$. The experiment was repeated in accordance with the preparation of thin BFO films in our previous experiments on the substrate surface of highly oriented pyrolytic graphite [12,13] and TiO_2 nanotubes [9,10]. In this work, Ta_2O_5/Si heterostructures were used as substrates [14] with thickness of Ta_2O_5 from 20 up to 100 nm. After obtaining the films, heat treatment was carried out in vacuum at temperature of 600 °C during 1 hour.

2.1 Atomic force microscopy data

AFM images of Ta_2O_5 with different thickness are given in Figure 1. The general tendency here is that the average surface roughness of the Ta_2O_5 layer grows with thickness. Right choice of scanning parameters [15-17] are important to obtain reliable results [18–22] with high resolution [23–26] to characterise the 3D surface microtexture and micromorphology [27-30].

Table 1 shows the characteristics of the AFM scanning in details.

Table 1. Parameters of AFM images acquisition.

Scanning probe microscope	Dimension Icon with Scan Asyst
Mode	ScanAsyst
Scan sizes	500 nm and 1 μ m
Aspect ratio	1
Scan rate	0.639 Hz
Samples/line	608
FeedBack Gain	from 17 to 19
Peak Force Set Point	477 pN
Peak Force Amplitude	150 nm
Peak Force Freq	2 kHz
Lift Height	25.1 nm
Sprint constant of Cantilever	0.4 N/m
Probe model	Scanasyst-air
Material	Silicon Tip on Nitride Lever
Tip Radius (Nom)	2 nm

Figure 1 shows the surface topography of the Ta₂O₅ layers depending on the thickness.

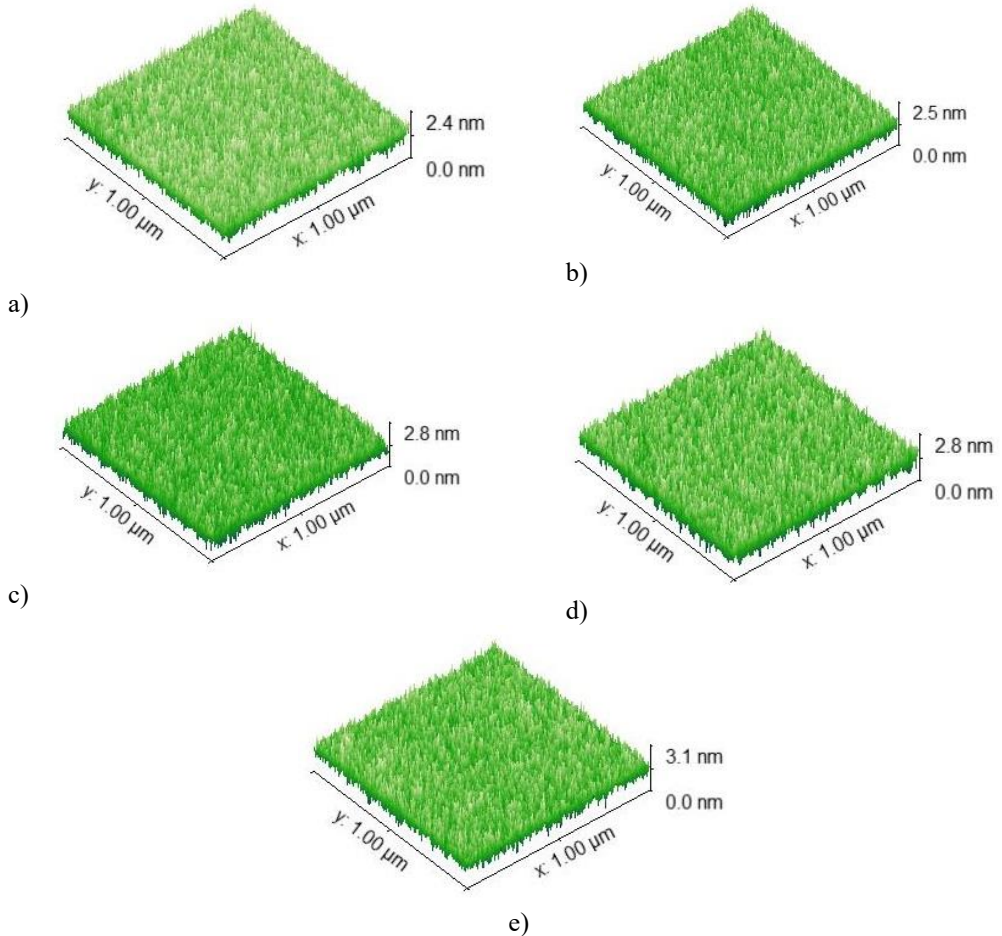


Fig. 1. Topography of Ta₂O₅ films with thickness of: a) 20 nm; b) 40 nm; c) 60 nm; d) 80 nm; e) 100 nm.

As shown in Figure 1, the topography of the film surface varies insignificantly depending on the thickness (from 20 nm to 100 nm): the difference of heights with a change of thickness (every 20 nm) is about 0.1 - 0.2 nm. A distinctive feature of hetero-epitaxial growth [31,32] is the formation of a pseudocubic structure of the resulting film due to the lattice mismatch between the substrate and the film. Such crystallization is typical for ion-plasma methods, where additional kinetic energy of the sprayed particles is involved. In the case of the ALD method, a chemical reaction occurs on the surface and only during heat treatment crystallites are formed on the surface. It was noted that thin Ta₂O₅ films were formed by the fractal mechanism [33]. This work also studied the correlation between the thickness of Ta₂O₅ thin films and their 3D micromorphology. Probably, thin BFO films repeat this growth mechanism at small thicknesses (~ 50 nm).

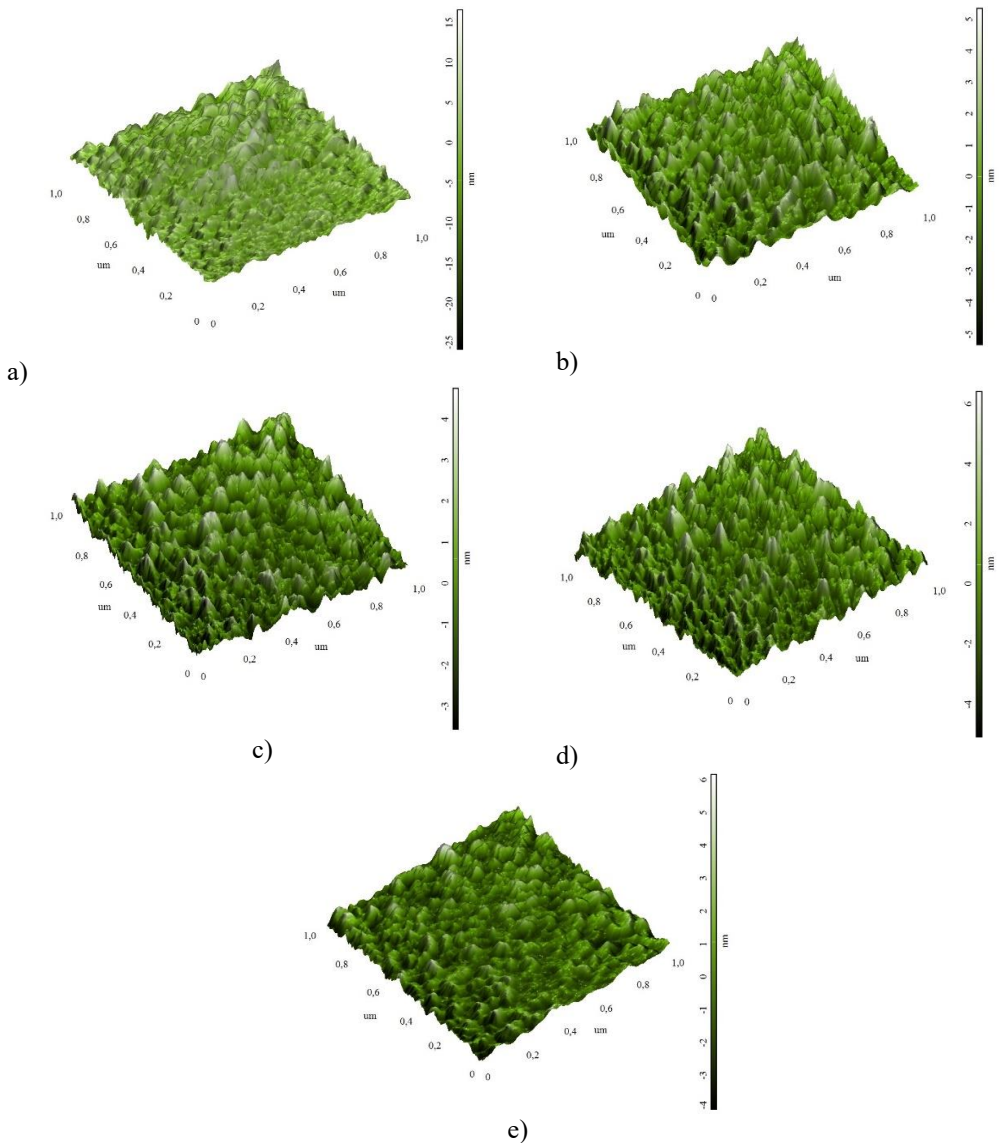


Fig. 2. Topography of the BFO film obtained on the surface of Ta₂O₅ layers with a thickness of: a) 20 nm; b) 40 nm; c) 60 nm; d) 80 nm; e) 100 nm

2.2 X-ray photoelectron spectroscopy data

The study of chemical conditions of the surface (5-10nm) was made by XPS (AXIS SupraTM). The XPS spectra of as-deposited BFO layers are given in Figure 3. Figure 4 contains spectra for the same layers after annealing procedure.

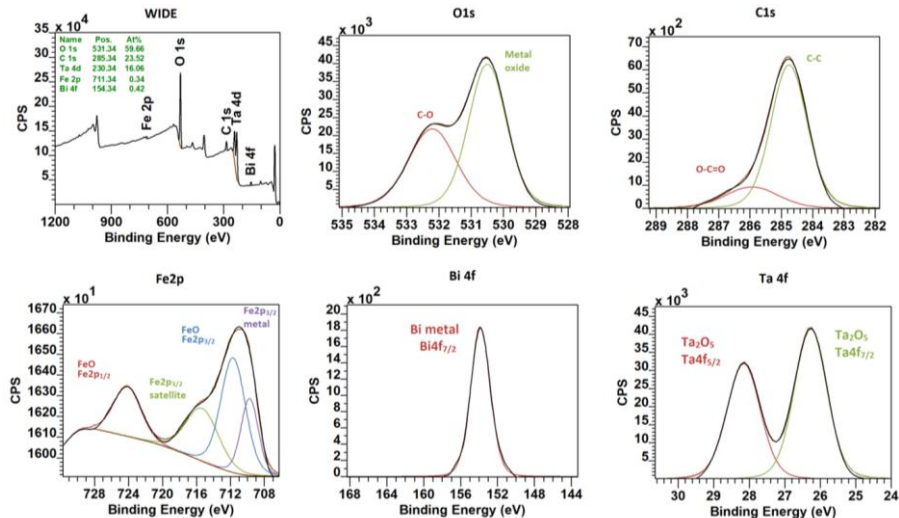


Fig. 3. XPS spectra of the deposited BFO films before annealing

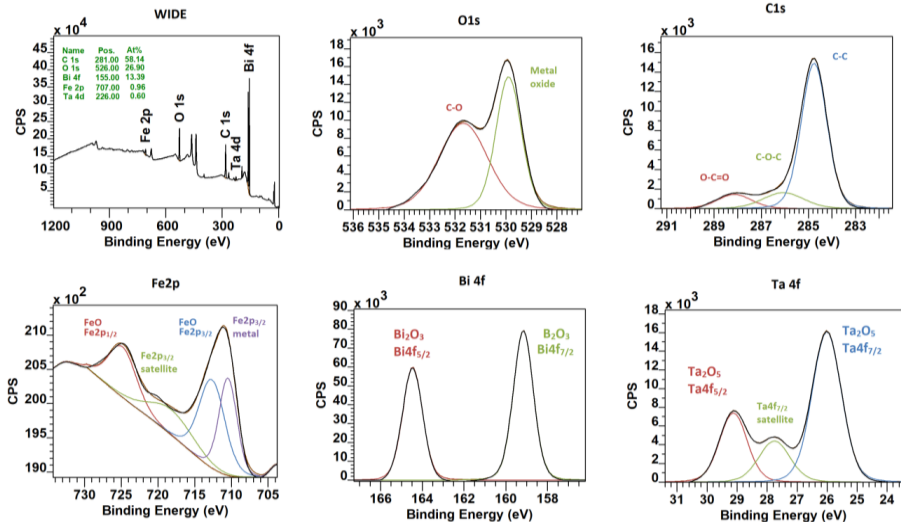


Fig. 4. XPS spectra of the deposited BFO films after annealing

By taking a look at the wide spectra of both as-deposited and annealed layers it can be inferred that the elemental ratio on the surface changes drastically after the annealing. The most noticeable change is the sharp decrease of the overall oxygen concentration. Another aspect worth mentioning is the increase of intensity of other elements such as Bi, Ta and Fe. The most plausible explanation to this is that the deposited samples had a few nm oxide layers on the surface. This oxide layer caused the overshadowing effect, due to which the high concentration of oxygen made other peaks appear low on the spectrum. Annealing,

apparently, removed the bulk of the surface oxide layer and the concentration profile has become more resembling of the actual concentration expected within the BFO layers. High resolution spectra provided in both figures also exhibit quite a bit of change. One can observe the change in the concentration of the certain bonds in the O1s and Fe2p spectra. C1s, Ta4f and Bi4f spectra on the other hand demonstrate formation/revelation of the entirely new bonds.

3 Conclusion

In this study BFO thin films were deposited on the surface of Ta₂O₅ with different thickness values. According to AFM, BFO films deposited on Ta₂O₅ layer with higher thickness also have higher values of the average surface roughness. Additionally, XPS analysis of the surface of BFO layers has been conducted. Spectra were demonstrated for as-deposited and annealed layers. According to the acquired data, as-deposited layer had a few nm oxide layers which was removed by to a large extent the annealing procedure.

Research described in this paper was financially supported by Internal Grant Agency of Brno University of Technology, grant No. FEKT-S-20-6352. CzechNanoLab project LM2018110 funded by MEYS CR is gratefully acknowledged for the financial support of the measurements/sample fabrication at CEITEC Nano Research Infrastructure.

References

- 1 X. Li, Y. Wang, F. Wang, A. Liang, *Mater. Lett.* **298**, 130000 (2021). <https://doi.org/10.1016/j.matlet.2021.130000>.
- 2 R. Wang, L. Pan, Q. Han, H. Zhu, M. Wan, Y. Mai, *J. Alloys Compd.* **865**, 158931 (2021). <https://doi.org/10.1016/j.jallcom.2021.158931>.
- 3 S. Das, V.K. Singh, *Photonics Nanostructures - Fundam. Appl.* **44**, 100904 (2021). <https://doi.org/10.1016/j.photonics.2021.100904>.
- 4 Y. Nishimura, A. Shinkawa, H. Ujita, M. Tsuji, M. Nakamura, *Appl. Surf. Sci.* **136**, 22–28 (1998). [https://doi.org/10.1016/S0169-4332\(98\)00332-8](https://doi.org/10.1016/S0169-4332(98)00332-8).
- 5 A.K. Narasimhan, S.L. Balasubramanian, G. Krishnamurthi, *Mater. Lett.* **300**, 130214 (2021). <https://doi.org/10.1016/j.matlet.2021.130214>.
- 6 Y. Ito, Y. Abe, M. Kawamura, K.H. Kim, T. Kiba, *Thin Solid Films.* **710**, 138276 (2020). <https://doi.org/10.1016/j.tsf.2020.138276>.
- 7 J. Zheng, K. Wen, Y. Liu, L. Gao, Z. Ma, X. Diao, *Ceram. Int.* **46**, 3875–3881 (2020). <https://doi.org/10.1016/j.ceramint.2019.10.113>.
- 8 L. Parshina, O. Novodvorsky, O. Khramova, D. Gusev, A. Polyakov, V. Mikhalevsky, E. Cherebilo, *Chaos, Solitons and Fractals.* **142** (2021). <https://doi.org/10.1016/j.chaos.2020.110460>.
- 9 F.F. Orudzhev, S.M. Ramazanov, A.B. Isaev, N.M. Alikhanov, D. Sobola, M.Y. Presniakov, *Mater. Today Proc.* 2018–2021 (2020). <https://doi.org/10.1016/j.matpr.2020.04.153>.
- 10 F. Orudzhev, S. Ramazanov, D. Sobola, A. Isaev, C. Wang, A. Magomedova, M. Kadiev, K. Kaviyarasu, *Nanomaterials.* **10**, 1–16 (2020). <https://doi.org/10.3390/nano10112183>.
- 11 B.G. Park, *Mater. Lett.* **285**, 129006 (2021). <https://doi.org/10.1016/j.matlet.2020.129006>.

- 12 S. Ramazanov, D. Sobola, F. Orudzhev, A. Knápek, J. Polčák, M. Potoček, P. Kaspar, R. Dallaev, *Nanomaterials*. **10**, 1–18 (2020). <https://doi.org/10.3390/nano10101990>.
- 13 D. Sobola, S. Ramazanov, M. Konečný, F. Orudzhev, P. Kaspar, N. Papež, A. Knápek, M. Potoček, *Materials (Basel)*. **13** (2020). <https://doi.org/10.3390/ma13102402>.
- 14 P. Kaspar, P. Škarvada, V. Holcman, L. Grmela, *Appl. Phys. A Mater. Sci. Process.* **125** (2019). <https://doi.org/10.1007/s00339-019-3134-3>.
- 15 A. Knápek, D. Sobola, D. Burda, A. Daňhel, M. Mousa, V. Kolařík, *Nanomaterials*. **9** (2019). <https://doi.org/10.3390/nano9121756>.
- 16 Ş. Țălu, R.P. Yadav, O. Šik, D. Sobola, R. Dallaev, S. Solaymani, O. Man, *Mater. Sci. Semicond. Process.* **85**, 15–23 (2018). <https://doi.org/10.1016/j.mssp.2018.05.030>.
- 17 N. Papež, A. Gajdoš, R. Dallaev, D. Sobola, P. Sedlák, R. Motúz, A. Nebojsa, L. Grmela, *Appl. Surf. Sci.* **510** (2020). <https://doi.org/10.1016/j.apsusc.2020.145329>.
- 18 A. Méndez, Y. Reyes, G. Trejo, K. Stepien, Ş. Țălu, *Microsc. Res. Tech.*, **78**, 1082 (2015)
- 19 Ş. Țălu, S. Stach, D. Raoufi, F. Hosseinpanahi, *Electron. Mater. Lett.*, **11**, 749 (2015)
- 20 A.R. Grayeli-Korpi, C. Luna, A. Arman, Ş. Țălu, *Results Phys*, **7**, 3349 (2017)
- 21 Ş. Țălu, S. Stach, A. Mahajan, D. Pathak, T. Wagner, A. Kumar, R.K. Bedi, M. Țălu, *Electron Mater Lett.*, **10**, 719 (2014)
- 22 Ş. Țălu, Z. Marković, S. Stach, B.T. Marković, M. Țălu, *Appl. Surf. Sci.*, **289**, 97 (2014)
- 23 D. Sobola, Ş. Țălu, S. Solaymani, L. Grmela, *Microsc. Res. Tech.*, **80**, 1328 (2017)
- 24 Ş. Țălu, I.A. Morozov, R.P. Yadav, *Appl Surf Sci.*, **484**, 892 (2019)
- 25 Ş. Țălu, A.J. Ghazai, S. Stach, H.A. Hassan, Z. Hassan, M. Țălu, *J. Mater. Sci. Mater. Electron.*, **25**, 466 (2014)
- 26 Ş. Țălu, *Micro and nanoscale characterization of three dimensional surfaces. Basics and applications*. (Napoca Star Publishing House, Cluj-Napoca, Romania, 2015).
- 27 Ş. Țălu, M. Bramowicz, S. Kulesza, V. Dalouji, S. Solaymani, S. Valedbagi, *Microsc. Res. Tech.*, **79**, 1208 (2016)
- 28 A. Jafari, M.H. Alam, D. Dastan, S. Ziakhodadadian, Z. Shi, H. Garmestani, A.S. Weidenbach, Ş. Țălu, *J Mater Sci: Mater Electron*, **30**, 21185 (2019)
- 29 A. Jafari, K. Tahani, D. Dastan, S. Asgary, Z. Shi, X.T. Yin, W.D. Zhou, H. Garmestani, Ş. Țălu, *Surf Interfaces*, **18**, article 100463 (2020)
- 30 Ş. Țălu, S. Stach, J. Zaharieva, M. Milanova, D. Todorovsky, S. Giovanzana, *Int J Polym Anal Ch.*, **19**, 404 (2014)
- 31 Ş. Țălu, S. Sebastian, R. Shikhgasan, S. Dinara, R. Guseyn, *Mater. Sci. Pol.* **35**, 539–547 (2017). <https://doi.org/10.1515/msp-2017-0049>.
- 32 S.M. Ramazanov, G.M. Ramazanov, *Tech. Phys. Lett.* **40**, 44–47 (2014). <https://doi.org/10.1134/S106378501401009X>.
- 33 D. Sobola, P. Kaspar, J. Oulehla, Ş. Țălu, N. Papež, *Mater. Sci. Pol.* (2020). <https://doi.org/10.2478/msp-2019-0083>.